INTERNATIONAL JOURNAL FOR NUMERICAL METHODS IN FLUIDS, VOL. 23, 163–176 (1996)

CONVECTIVE HEAT TRANSFER FROM A CIRCULAR CYLINDER UNDER THE EFFECT OF A SOLID PLANE WALL

YUE-TZU YANG, CHA'O-KUANG CHEN AND CHI-FANG CHIU

Department of Mechanical Engineering, National Cheng-Kung University, Tainan, Taiwan

SUMMARY

The purpose of this investigation is to study the convective heat transfer from a horizontal circular cylinder under the effect of a solid plane wall. The full Navier–Stokes and energy equations for two-dimensional steady flow are solved by a finite element method. The variations in surface shear stress, local pressure and Nusselt number around the surface of the cylinder as well as the predicted values of average Nusselt number, location of separation and some flow and temperature fields are presented. It is found that the average Nusselt number and drag force increase as the gap between the cylinder and the wall is increased.

KEY WORDS: convective heat transfer; finite element method

INTRODUCTION

Heat transfer from a horizontal circular cylinder continues to be one of the important engineering problems. Many investigations[1–9] have been carried out to study the combined forced and natural convection heat transfer from a circular cylinder, but the influence of a neighbouring solid wall on the heat transfer from the cylinder has rarely been considered. In engineering applications, most heat exchanger pipes do not exist alone and always experience a certain degree of influence from neighbouring bodies. The present paper investigates the effect of a neighbouring wall on the convective heat transfer from an isothermal cylinder in a viscous incompressible fluid.

Flow past an obstacle under the effect of a solid wall has been analysed mostly by two approaches. One is based on the Stokes equations of motion.[10] The other uses matched asymptotic expansions and treats the outer region as an ideal inviscid flow.[11,12] However, each method needs some additional assumptions and suffers from certain limitations. Many papers have focused attention primarily on the flow field and little attention is given to the heat transfer characteristics. In the present paper a Galerkin finite element method is employed to solve the full Navier–Stokes and energy equations. The effects of the plane wall as well as the Reynolds number and Grashof number on the heat transfer are of particular interest.

PROBLEM STATEMENT

Consider an incompressible viscous fluid of temperature T_∞ streaming uniformly towards an infinite adiabatic plane wall behind an infinite isothermal cylinder of diameter D and temperature T_w. The computation domain, boundary conditions and co-ordinate system of the flow field are shown in Figure 1. Far away from the cylinder, zero gradient is assumed.

CCC 0271–2091/96/020163–14

Received May 1995
Revised November 1995

Owing to small changes in the temperature, all fluid property variations are ignored except for density in the buoyancy term in the momentum equation. The dimensionless governing equations can be written as follows: continuity equation

$$\frac{\partial u}{\partial x}+\frac{\partial v}{\partial y}=0, \tag{1}$$

momentum equations

$$u\frac{\partial u}{\partial x}+v\frac{\partial u}{\partial y}=-\frac{\partial p}{\partial x}+\frac{1}{Re}\left(\frac{\partial^2 u}{\partial x^2}+\frac{\partial^2 u}{\partial y^2}\right)+\frac{Gr}{Re^2}\phi, \tag{2}$$

$$u\frac{\partial v}{\partial x}+v\frac{\partial v}{\partial y}=-\frac{\partial p}{\partial y}+\frac{1}{Re}\left(\frac{\partial^2 v}{\partial x^2}+\frac{\partial^2 v}{\partial y^2}\right), \tag{3}$$

energy equation

$$u\frac{\partial \phi}{\partial x}+v\frac{\partial \phi}{\partial y}=\frac{1}{Pe}\left(\frac{\partial^2 \phi}{\partial x^2}+\frac{\partial^2 \phi}{\partial y^2}\right), \tag{4}$$

where

$$u=\frac{u^*}{U_\infty}, \qquad v=\frac{v^*}{U_\infty}, \qquad \phi=\frac{T^*-T_\infty}{T_w-T_\infty},$$

$$P=\frac{P^*-P_\infty}{\rho U_\infty^2}, \qquad x=\frac{x^*}{D}, \qquad y=\frac{y^*}{D},$$

$$Gr=\frac{g\beta(T_w-T_\infty)D^3}{\nu^2}.$$

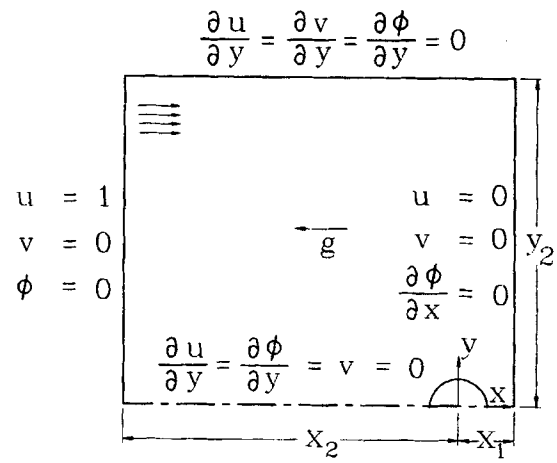

Figure 1. Computation domain and boundary conditions

FINITE ELEMENT METHOD

The calculated flow domain is discretized into 230–271 elements, determined by the size of the gap between the cylinder and the plane wall. All the elements are isoparametric quadrilateral containing eight nodes, one at each corner and one at the midpoint of each side. The method of mixed interpolation presented by Hood and Taylor[13] is adopted with quadratic variations in velocity and temperature and linear variation in pressure within the element; that is, all eight nodes are associated with velocities and temperature but only the corner nodes with pressure in the same element. Thus

$$u = \sum_{j=1}^{8} N_j u_j, \qquad v = \sum_{j=1}^{8} N_j v_i, \qquad \phi = \sum_{j=1}^{8} N_j \phi_j, \qquad P = \sum_{l=1}^{4} M_l P_l, \tag{5}$$

where N_j is the shape function of velocities and temperature and M is the shape function of pressure. By employing the Galerkin weighted residual approach, equations (1)–(4) can be discretized as follows: continuity equation

$$\sum_{1}^{n_e} \int_{A^e} M_l \left(\frac{\partial N_j}{\partial x} u_j + \frac{\partial N_j}{\partial y} v_j \right) \mathrm{d}A^e = 0, \tag{6}$$

momentum equations

$$\sum_{1}^{n_e} \int_{A^e} \left[\left(N_i N_k u_k \frac{\partial N_j}{\partial x} u_j + N_i N_k v_k \frac{\partial N_j}{\partial y} u_j + N_i \frac{\partial M_l}{\partial x} P_l \right) + \frac{1}{Re} \left(\frac{\partial N_i}{\partial x} \frac{\partial N_j}{\partial x} u_j + \frac{\partial N_i}{\partial y} \frac{\partial N_j}{\partial y} u_j \right) - \frac{Gr}{Re^2} N_i N_j \phi_j \right] \mathrm{d}A^e - \int_{\Gamma_1} \frac{1}{Re} N_i \frac{\partial N_j}{\partial n} u_j \mathrm{d}\Gamma - \int_{\Gamma_2} \frac{1}{Re} N_i \frac{\partial u}{\partial n} \mathrm{d}\Gamma = 0, \tag{7}$$

$$\sum_{1}^{n_e} \int_{A^e} \left[\left(N_i N_k u_k \frac{\partial N_j}{\partial x} v_j + N_i N_k v_k \frac{\partial N_j}{\partial y} v_j + N_i \frac{\partial M_l}{\partial y} P_l \right) + \frac{1}{Re} \left(\frac{\partial N_i}{\partial x} \frac{\partial N_j}{\partial x} v_j + \frac{\partial N_i}{\partial y} \frac{\partial N_j}{\partial y} v_j \right) \right] \mathrm{d}A^e - \int_{\Gamma_1} \frac{1}{Re} N_i \frac{\partial N_j}{\partial n} v_j \mathrm{d}\Gamma - \int_{\Gamma_2} \frac{1}{Re} N_j \frac{\partial v}{\partial n} \mathrm{d}\Gamma = 0, \tag{8}$$

energy equation

$$\sum_{1}^{n_e} \int_{A^e} \left[\left(N_i N_k u_k \frac{\partial N_j}{\partial x} \phi_j + N_i N_k v_k \frac{\partial N_j}{\partial y} \phi_j \right) + \frac{1}{Pe} \left(\frac{\partial N_i}{\partial x} \frac{\partial N_j}{\partial x} \phi_j + \frac{\partial N_i}{\partial y} \frac{\partial N_j}{\partial y} \phi_j \right) \right] \mathrm{d}A^e - \int_{\Gamma_1} \frac{1}{Pe} N_i \frac{\partial N_j}{\partial n} \phi_j \mathrm{d}\Gamma - \int_{\Gamma_2} \frac{1}{Pe} N_j \frac{\partial v}{\partial n} \mathrm{d}\Gamma = 0, \tag{9}$$

where $l = 1, 2, 3, 4$, $i = 1, 2, 3, \ldots, 8$, $j = 1, 2, 3, \ldots, 8$, $A^e =$ is the area of a single element, $\Gamma_2 =$ is the boundary over which the normal gradient is specified and Γ_1 is the rest of the boundary excluding Γ_2. The assembled matrix equation is in the form

$$A\lambda = B, \tag{10}$$

where the primitive variables for λ are

$$\lambda_j = \begin{Bmatrix} u_j \\ p_j \\ v_j \\ \phi_j \end{Bmatrix}. \tag{11}$$

The coefficients in the matrix A are

$$a_{ij} = \sum_{1}^{n_e} \int_{A^e} \begin{bmatrix} C_{11} & C_{12} & C_{13} & C_{14} \\ C_{21} & C_{22} & C_{23} & C_{24} \\ C_{31} & C_{32} & C_{33} & C_{34} \\ C_{41} & C_{42} & C_{43} & C_{44} \end{bmatrix} dA^e - \sum_{1}^{n_e} \int_{\Gamma_1} \begin{bmatrix} \frac{1}{Re} N_i \frac{\partial N_j}{\partial n} & 0 & 0 & 0 \\ 0 & 0 & 0 & 0 \\ 0 & 0 & \frac{1}{Re} N_i \frac{\partial N_j}{\partial n} & 0 \\ 0 & 0 & 0 & \frac{1}{Pe} N_i \frac{\partial N_j}{\partial n} \end{bmatrix} d\Gamma, \quad (12)$$

where

$$C_{11} = N_i N_k u_k \frac{\partial N_j}{\partial x} + N_i N_k v_k \frac{\partial N_j}{\partial y} + \frac{1}{Re}\left(\frac{\partial N_i}{\partial x}\frac{\partial N_j}{\partial x} + \frac{\partial N_i}{\partial y}\frac{\partial N_j}{\partial y}\right),$$

$$C_{12} = N_i \frac{\partial M_l}{\partial x}, \qquad C_{13} = 0, \qquad C_{14} = -\frac{Gr}{Re^2} N_i N_j,$$

$$C_{21} = M_l \frac{\partial N_j}{\partial x}, \qquad C_{22} = 0, \qquad C_{23} = M_l \frac{\partial N_j}{\partial y}, \qquad C_{24} = 0,$$

$$C_{31} = 0, \qquad C_{32} = N_i \frac{\partial M_l}{\partial y}, \qquad C_{33} = C_{11}, \qquad C_{34} = 0,$$

$$C_{41} = 0, \qquad C_{42} = 0, \qquad C_{43} = 0,$$

$$C_{44} = N_i N_k u_k \frac{\partial N_j}{\partial x} + N_i N_k v_k \frac{\partial N_j}{\partial y} + \frac{1}{Pe}\left(\frac{\partial N_i}{\partial x}\frac{\partial N_j}{\partial x} + \frac{\partial N_i}{\partial y}\frac{\partial N_j}{\partial y}\right).$$

The coefficients in the matrix B are

$$b_{ij} = \int_{\Gamma_2} \begin{bmatrix} b_1 \\ b_2 \\ b_3 \\ b_4 \end{bmatrix} d\Gamma, \quad (13)$$

where

$$b_1 = \frac{1}{Re} N_i \frac{\partial u}{\partial n}, \qquad b_2 = 0, \qquad b_3 = \frac{1}{Re} N_i \frac{\partial v}{\partial n}, \qquad b_4 = \frac{1}{Pe} N_i \frac{\partial \phi}{\partial n}.$$

NUMERICAL SOLUTION

In the above formulation, all integrations are performed by using the Gauss–Legendre quadrature scheme. In the present work, 3 × 3 and 3 × 1 Gaussian integration sampling point schemes are used for the surface and line integrals respectively. The resultant non-linear matrix equations are solved by the frontal method presented by Irons[14] and a Newton–Raphson iterative process is carried out to speed up the rate of convergence. The relaxation factor $\alpha = 0{\cdot}5$ was employed to promote smooth convergence. The following convergence criterion was used for the computation:

$$\left| \frac{\phi^{n+1} - \phi^n}{\phi^{n+1}} \right| < 0 \cdot 001, \quad (14)$$

where ϕ represents U, V or T and n is the iteration number. All computations were executed on a PC486. The programme converged in about 5500 CPU seconds.

CALCULATION OF PHYSICAL PARAMETERS

Shear stress

The shear stress is defined as

$$\tau_w^* = \mu \frac{\partial U_t^*}{\partial n^*} = \frac{\mu U_\infty}{D} \frac{\partial U_t}{\partial n}, \tag{15}$$

where $U_t = U_t^*/U_\infty$, $n = n^*/D$ and $\partial U_t/\partial n$ denotes the dimensionless gradient of tangential velocity in the direction normal to the cylinder surface. Thus the dimensionless shear stress is defined as

$$\tau_w = \frac{\tau_w^*}{\rho U_\infty^2} = \frac{\mu}{\rho U_\infty D} \frac{\partial U_t}{\partial n} = \frac{1}{Re} \frac{\partial U_t}{\partial n}. \tag{16}$$

Nusselt number

From the energy balance at the cylinder surface one has

$$-K(\nabla^* T \cdot n)_w = h(T_w - T_\infty) \quad \text{or} \quad -K \frac{1}{D} (\nabla \phi \cdot n)_w = h. \tag{17}$$

The local Nusselt number can then be written as

$$Nu = \frac{hD}{K} = -(\nabla \phi \cdot n)_w = -\frac{\partial \phi}{\partial n_w} = -\frac{\partial N_j}{\partial n} \phi_j. \tag{18}$$

The average Nusselt number is defined as

$$\overline{Nu} = \frac{1}{\pi} \int_0^\pi Nu \, d\theta. \tag{19}$$

RESULTS AND DISCUSSION

It can be seen from the governing equations (1)–(4) that the heat transfer characteristics of a hot horizontal cylinder under the effect of a neighbouring solid plane wall depend on the Reynolds number, Prandtl number, Grashof number and the gap between the cylinder and the plane wall. In the present paper the fluid is assumed to be a gas with a Prandtl number of 0·7.

It can be seen from Figure 2(a)–(c) that the local Nusselt number and dimensionless shear stress around the cylinder surface increase when the gap is increased but that the dimensionless pressure decreases. The influence of the neighbouring wall seems to reduce the velocity of the flow and force it to stream sidewards along the plane wall. The velocity reduction results in a decrease in the heat transfer rate and surface shear stress on the cylinder and thus there is a decrease in the local Nusselt number and drag force but an increase in the pressure on the cylinder. Also, the smaller the gap x_1/D is, the stronger are the effects of the velocity deceleration. In addition, the local Nusselt number distribution presented in Figure 2(a) is seen to agree well with the result of Dennis and Chang.[6]

The effect of the Reynolds number on the average Nusselt number in the forced convection situation is shown in Figure 3. It is clear that the greater *Re* is, the greater is *Nu*. The effects of the Reynolds number on the local Nusselt number, dimensionless shear stress and dimensionless pressure distributions around the cylinder are shown in Figure 4(a)–(c) respectively. It is seen that an increase in the Reynolds number tends to increase the local Nusselt number as well as the surface shear stress but tends to decrease the surface pressure.

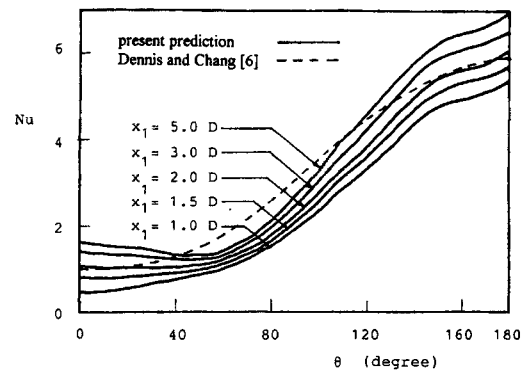

Figure 2(a). Local Nusselt number distributions for $Re = 100$ and $Gr = 0$

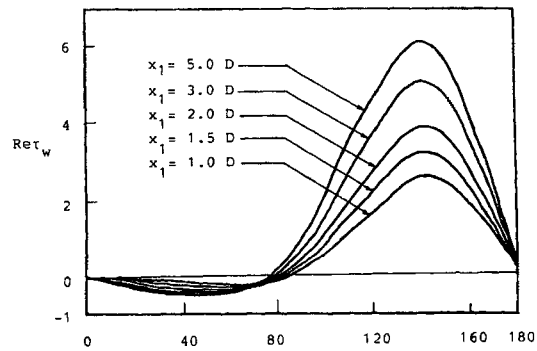

Figure 2(b). Dimensionless surface shear stress distributions for $Re = 100$ and $Gr = 0$

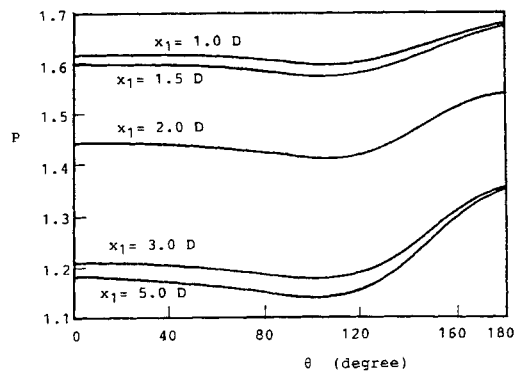

Figure 2(c). Dimensionless surface pressure distributions for $Re = 100$ and $Gr = 0$

The parameter Gr/Re^2 is found to have a great influence on the velocity and thermal fields. The variations in average Nusselt number for $Re = 100$ and different values of Gr are shown in Figure 5. It is clear from this figure that Nu increases with an increase in Gr. Figure 6(a)–(c) show the variations in local Nusselt number, dimensionless surface shear stress and surface pressure respectively for $Re = 100$ and different values of Gr. It can be seen that an increase in Gr trends to increase the local Nusselt number and surface shear stress but to decrease the surface pressure significantly.

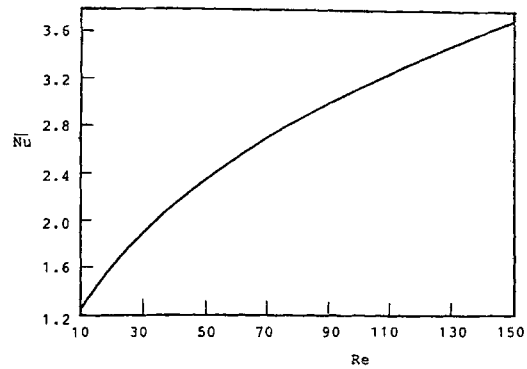

Figure 3. Effect of Re on average Nusselt number for $x_1/D = 3{\cdot}0$ and $Gr = 0$

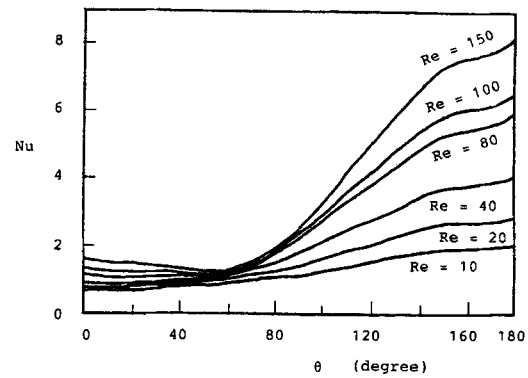

Figure 4(a). Local Nusselt number distributions for $x_1/D = 3{\cdot}0$ and $Gr = 0$

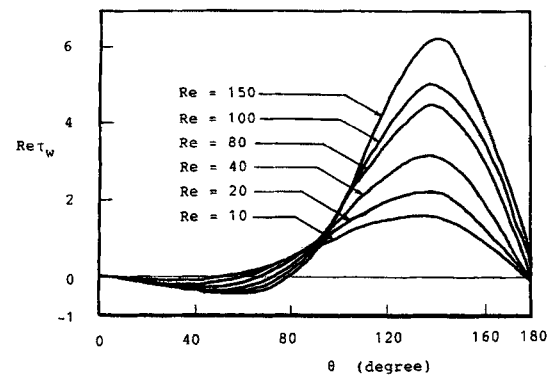

Figure 4(b). Dimensionless surface shear stress distributions for $x_1/D = 3{\cdot}0$ and $Gr = 0$

The isotherms for different gap sizes are shown in Figure 7(a)–(d). It is clear from these figures that the isotherms near the front stagnation point are closer than those near the rear stagnation point. Closer isothermal lines indicate a higher temperature gradient and accordingly a higher heat transfer rate. The influence of the solid plane wall is also significant in the rear region and a higher heat transfer rate for the bigger-gap case is indicated. The isotherms at $x_1/D = 3{\cdot}0$ for different values of Re are shown in

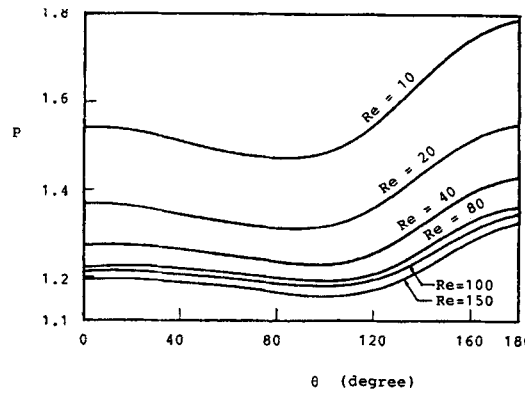

Figure 4(c). Dimensionless surface pressure distributions for $x_1/D = 3{\cdot}0$ and $Gr = 0$

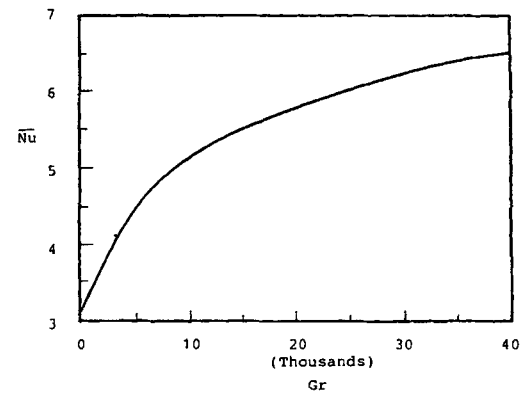

Figure 5. Effect of Gr on average Nusselt number for $x_1/D = 3{\cdot}0$ and $Re = 0$

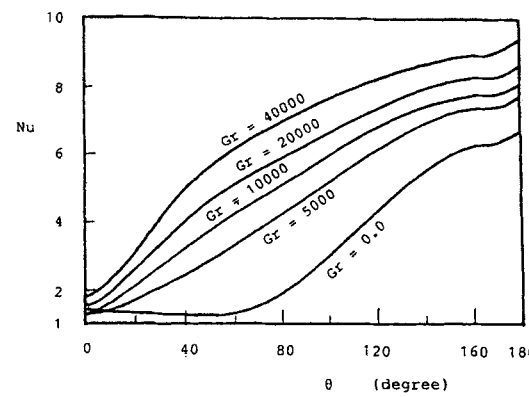

Figure 6(a). Local Nusselt number distributions for $x_1/D = 3{\cdot}0$ and $Re = 100$

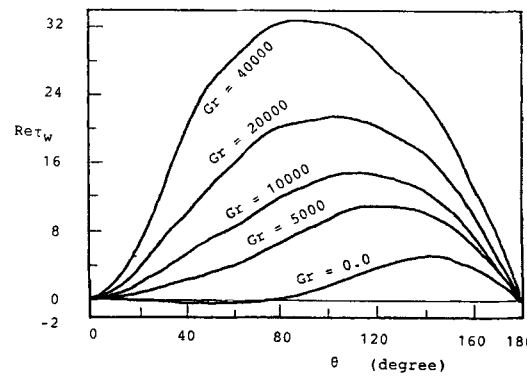

Figure 6(b). Dimensionless surface shear stress distributions for $x_1/D = 3{\cdot}0$ and $Re = 100$

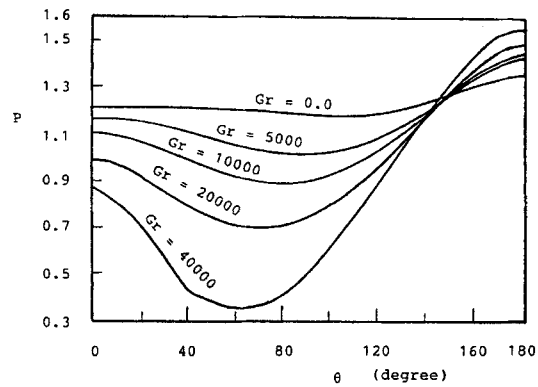

Figure 6(c). Dimensionless surface pressure distributions for $x_1/D = 3{\cdot}0$ and $Re = 100$

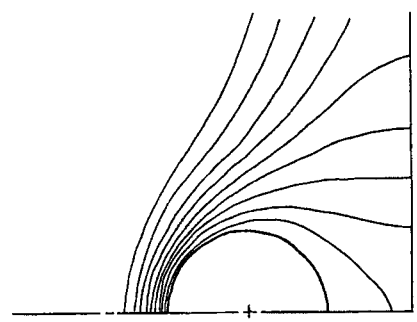

Figure 7(a). Isotherms at $x_1/D = 1{\cdot}0$, $Re = 100$ and $Gr = 0$

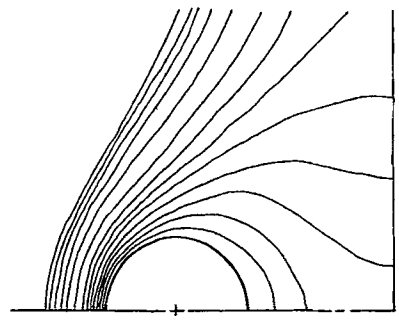

Figure 7(b). Isotherms at $x_1/D = 1{\cdot}5$, $Re = 100$ and $Gr = 0$

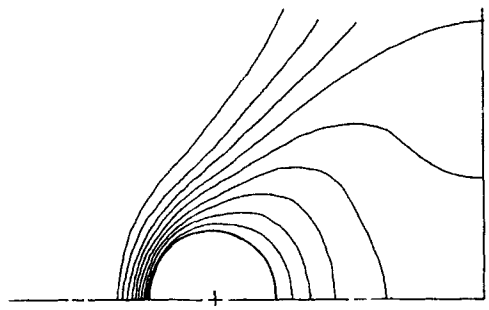

Figure 7(c). Isotherms at $x_1/D = 2{\cdot}0$, $Re = 100$ and $Gr = 0$

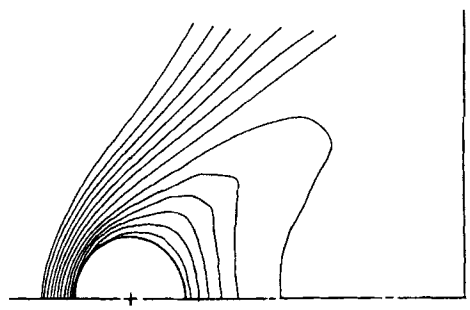

Figure 7(d). Isotherms at $x_1/D = 3{\cdot}0$, $Re = 100$ and $Gr = 0$

Figure 8(a) and 8(b). From these figures it is found that as Re increases, the isothermal lines get closer to the cylinder surface. The velocity fields and isotherms at $x_1/D = 3{\cdot}0$ for different values of Gr/Re^2 are shown in Figure 9(a)–(c) and 10(a)–(c). It can be seen that as Gr increases, a significant acceleration of the flow velocity behind the cylinder occurs and the isothermal lines around the cylinder get closer and shift towards the plane wall.

Table I gives a comparison of average Nusselt numbers for different extents of the physical domain. It is found that the location of the inflow boundary has a significant influence on the computational results. The main reason for the difference is the restrictive imposition of too rapid a deceleration, which is incompatible with the far-field condition being simulated. However, a far-field computation domain can hardly be achieved owing to the limitation of computation time.

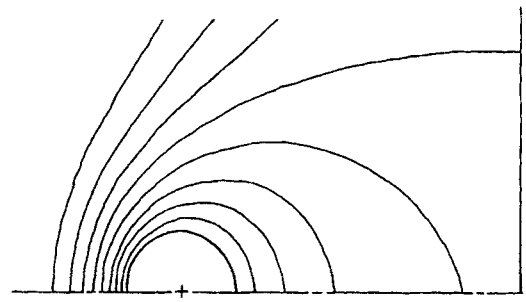

Figure 8(a). Isotherms at $x_1/D = 3{\cdot}0$, $Re = 10$ and $Gr = 0$

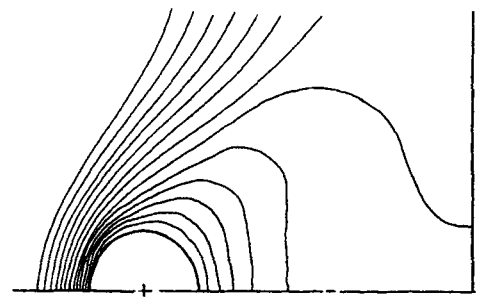

Figure 8(b). Isotherms at $x_1/D = 3{\cdot}0$, $Re = 80$ and $Gr = 0$

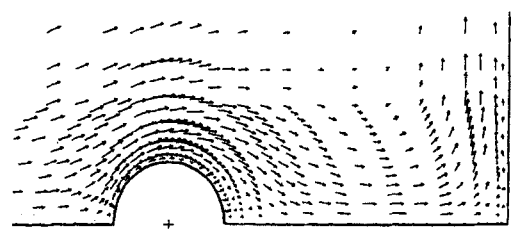

Figure 9(a). Velocity field at $x_1/D = 3{\cdot}0$, $Re = 100$ and $Gr = 5000$

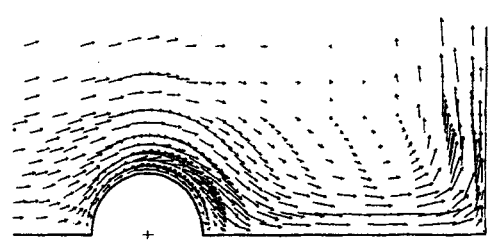

Figure 9(b). Velocity field at $x_1/D = 3{\cdot}0$, $Re = 100$ and $Gr = 20{,}000$

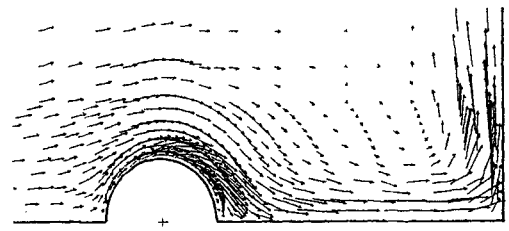

Figure 9(c). Velocity field at $x_1/D = 3{\cdot}0$, $Re = 100$ and $Gr = 40{,}000$

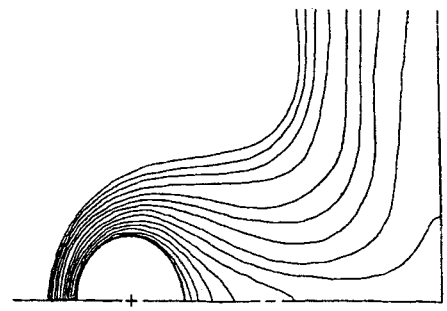

Figure 10(a). Isotherms at $x_1/D = 3{\cdot}0$, $Re = 100$ and $Gr = 5000$

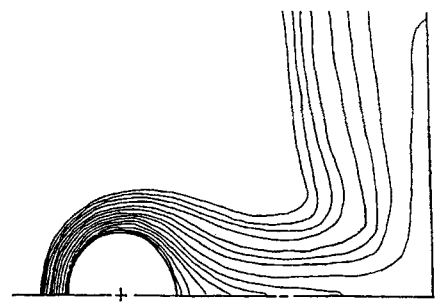

Figure 10(b). Isotherms at $x_1/D = 3{\cdot}0$, $Re = 100$ and $Gr = 20{,}000$

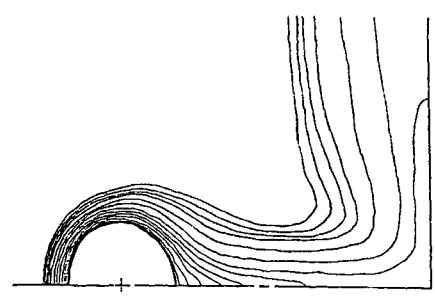

Figure 10(c). Isotherms at $x_1/D = 3{\cdot}0$, $Re = 100$ and $Gr = 40{,}000$

Table I. Comparison of average Nusselt numbers for different extents of physical domain ($Re = 100$; $Gr = 0$; N_{elem}, number of elements)

x_1/D	x_2/D	y_2/D	N_{elem}	$\overline{Nu}$
3·0	8·5	8·0	242	3·13533
3·0	13·5	8·0	293	3·0221
3·0	8·5	12·5	266	3·1365

CONCLUSIONS

A finite element solution based on the full Navier–Stokes and energy equations for an isothermal circular cylinder under the effect of a solid plane wall is obtained. Both forced convection and mixed convection are considered. The effects of Reynolds number, Grashof number and the neighbouring plane wall on the flow and heat transfer characteristics around the circular cylinder are discussed in detail. It is found that an increase in the parameter Gr/Re^2 has an accelerating effect and the presence of a neighbouring plane wall has a decelerating effect on the flow around the cylinder. Accordingly, the heat transfer rate and drag force increase with increasing gap size and Grashof number. The velocity fields and isotherms for different cases are also presented to show details of the flow and heat transfer characteristics. All results are reasonable in a physical sense.

APPENDIX: NOMENCLATURE

A global coefficient matrix
a_{ij} element of global coefficient matrix
B natural boundary condition vector
b_j element of natural boundary condition vector
C_{ij} element of coefficient matrix of single element
C_p specific heat at constant pressure
D diameter of cylinder
Gr Grashof number
g gravitational acceleration
h local heat transfer coefficient
K thermal conductivity
M shape function of four nodes
N_i shape function of eight nodes
Nu local Nusselt number
$\overline{Nu}$ average Nusselt number
n_e total element number
n normal vector of the boundary
p^* pressure
p dimensionless pressure, $p^*/\rho U_\infty^2$
Pe Peclet number, $Pr\,Re$
Pr Prandtl number, $\mu C_p/K$
Re Reynolds number, $\rho U_\infty D/\mu$
T^* temperature
T_w temperature on cylinder surface
T_∞ freestream temperature

u^*, v^* x- and y-component of velocity
u, v dimensionless x- and y-component of velocity
u_j x-velocity component of node j
U_∞ freestream velocity
v_j y-velocity component of node j
X transverse axis of Cartesian co-ordinate
X_1 distance between centre of cylinder and wall
x^*, y^* x- and y-co-ordinate
x, y dimensionless x- and y-co-ordinate
Y Cartesian co-ordinate

Greek letters

β coefficient of volumetric thermal expansion
Γ boundary of flow domain
Γ_1 boundary with fixed value boundary condition
Γ_2 boundary with natural boundary condition
θ plane angle
λ primitive variable vector
μ dynamic viscosity
ν kinematic viscosity
ρ density of fluid
τ_w^* surface shear stress
τ_w dimensionless surface shear stress
ϕ dimensionless temperature, $(T^* - T_\infty)/(T_w - T_\infty)$
ϕ_j temperature of node j

REFERENCES

1. N. D. Joshi and S. P. Sukhatme, 'An analysis of combined free and forced convection heat transfer from a horizontal circular cylinder to a transverse flow', *J. Heat Transfer*, **93**, 441–448 (1971).
2. S. Nakai and T. Okazaki, 'Heat transfer from a horizontal circular cylinder wire at small Reynolds and Grashof number—II', *Int. J. Heat Mass Transfer*, **18**, 397–413 (1975).
3. E. M. Sparrow and L. Lee, 'Analysis of mixed convection about a horizontal cylinder', *Int. J. Heat Mass Transfer*, **19**, 229–232 (1976).
4. J. H. Merkin, 'Mixed convection from a horizontal circular cylinder', *Int. J. Heat Mass Transfer*, **20**, 73–77 (1976).
5. A. Mucoglu and T. S. Chen, 'Analysis of combined force and free convection cross a horizontal cylinder', *Can. J. Chem. Eng.*, **55**, 265–271 (1977).
6. S. C. R. Dennis and G. Chang, 'Numerical solutions for steady flow past circular cylinder at Reynolds numbers up to 100', *J. Fluid Mech.*, **42**, 471–489 (1970).
7. H. M. Badr, 'Laminar combined convection from a horizontal cylinder—parallel and contra flow regimes', *Int. J. Heat Mass Transfer*, **27**, 15–27 (1984).
8. A. P. Hatton, D. D. James and H. W. Swire, 'Combined forced and natural convection with low-speed air flow over horizontal cylinder', *J. Fluid Mech.*, **42**, 17–31 (1970).
9. B. Gebhart and L. Pera, 'Mixed convection from long horizontal cylinders', *J. Fluid Mech.*, **45**, 49–64 (1970).
10. A. M. J. Davis and M. E. O'Neill, 'Separation in a slow linear flow past a cylinder and a plane', *J. Fluid Mech.*, **80**, 551–564 (1977).
11. Z. Zapryanov and I. Lambova, 'Boundary layer growth on a circular cylinder in a semi-infinite fluid', *J. Appl. Math. Phys. (ZAMP)*, **37**, 176–193 (1986).
12. C.-Y. Wang, 'Separation and stall of an impulsively started elliptic cylinder', *J. Appl. Mech.*, **34**, 823–828 (1967).
13. P. Hood and C. Taylor, 'Navier–Stokes equations using mixed interpolation', *Proc. 1st Int. Conf. on F.E.M. in Fluid Problems*, Pineridge, Swansea, 1974.
14. B. M. Irons, 'A frontal solution program for finite element analysis', *Int. j. numer. methods eng.*, **12**, 5–32 (1970).